



Cite this: *Org. Biomol. Chem.*, 2017, **15**, 8655

Received 12th September 2017,
Accepted 28th September 2017

DOI: 10.1039/c7ob02289a

rsc.li/obc

Synthesis of kinase inhibitors containing a pentafluorosulfanyl moiety†

Supojjanee Sansook,^{‡a} Cory A. Ocasio,^{ib} a Iain J. Day,^{ib} a Graham J. Tizzard,^{ib} b Simon J. Coles,^{ib} b Oleg Fedorov,^c James M. Bennett,^d Jonathan M. Elkins^{ib} d and John Spencer^{ib} *a

A series of 3-methylidene-1*H*-indol-2(3*H*)-ones substituted with a 5- or 6-pentafluorosulfanyl group has been synthesized by a Knoevenagel condensation reaction of SF₅-substituted oxindoles with a range of aldehydes. The resulting products were characterized by X-ray crystallography studies and were tested for biological activity *versus* a panel of cell lines and protein kinases. Some exhibited single digit nM activity.

Introduction

The dysregulation of protein phosphorylation mediated by protein kinases is key to the progression of a number of cancers. Unsurprisingly, a number of ATP-competitive kinase inhibitors are in clinical use and development.^{1–7} For example, the oxindole-containing antiangiogenic drug Sunitinib **1**, containing a 5-fluorine substituent and a solubilizing side chain on the pyrrole unit, is in clinical use and superseded Semaxanib (**2**, SU5416) (Fig. 1) as well as inspiring a number of other studies on druglike oxindoles.^{8–15}

Metal-based analogues such as **3**, **4** have been described by our group and show kinase inhibition down to the nM range and tolerance of a range of substituents at the C-5 position.^{16,17}

Meggers's group replaced the sugar unit in staurosporine, a pan-kinase inhibitor with relatively high toxicity and unsuitable for clinical use, by square planar and octahedral transition metal complexes **5–7**, leading to highly potent, selective kinase inhibitors. This was attributed to the novel “imaginary hypervalent carbon” geometry enabled by the metal complexes (Fig. 2, **5–7**).^{18–21}

The pentafluorosulfanyl group is attracting increasing interest in medicinal chemistry. Displaying strong polarity, high



Fig. 1 Oxindole-based kinase inhibitors.

lipophilicity and good stability under physiological conditions, an SF₅ substituent has often been shown to behave like a CF₃ group.^{22–26} Here we show that a SF₅ group can be incorporated in both classical and metal-based oxindole derivatives, at the 5- or 6-position, leading to analogues displaying kinase inhibition down to the nM range.

Results and discussion

Microwave-mediated Knoevenagel condensations of the commercially-available 5- or 6-SF₅-substituted oxindoles **8**²⁷ with three separate aldehydes led to the products **10–14** (Scheme 1).²⁸

The structures of the pyrrole-containing positional isomers **10** and **11** were confirmed by ¹H NMR, ¹³C NMR spectroscopy, elemental analysis and mass spectrometry. In their ¹H NMR spectra the most downfield signals were assigned to the pyrrole-NH groups (δ 11.10–13.40 ppm) due to an intra-

^aDept of Chemistry, School of Life Sciences, University of Sussex, Falmer, BN1 9QJ, UK. E-mail: j.spencer@sussex.ac.uk

^bUK National Crystallography Service, Chemistry, University of Southampton, Highfield, Southampton, SO17 1BJ, UK

^cStructural Genomics Consortium, Nuffield Department of Clinical Medicine, University of Oxford, Oxford, OX3 7DQ, UK

^dStructural Genomics Consortium, Universidade Estadual de Campinas, Campinas, SP 13083-886, Brazil

†Electronic supplementary information (ESI) available. CCDC 154150–154153. For ESI and crystallographic data in CIF or other electronic format see DOI: 10.1039/c7ob02289a

[‡]Faculty of Science and Technology, Princess of Naradhiwas University, Thailand 96000.



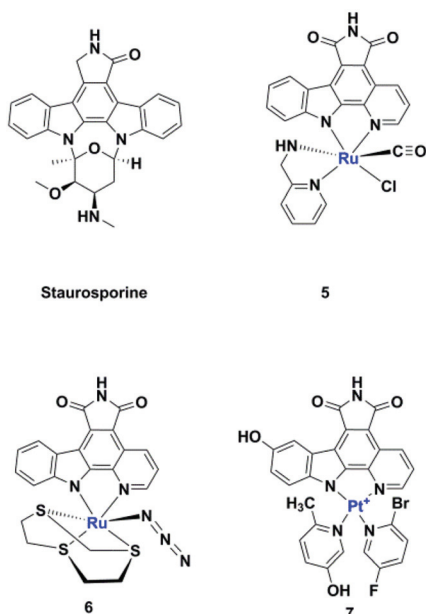


Fig. 2 Staurosporine analogues.



Scheme 1 Microwave-mediated Knoevenagel condensations.

molecular NH...O=C hydrogen bond and further confirmation of their anticipated Z-configuration and such a hydrogen bond was provided in the solid state (Fig. 3).²⁹

The related reaction with ferrocene carboxaldehyde afforded a mixture of stereoisomers 12a and 12b, which were

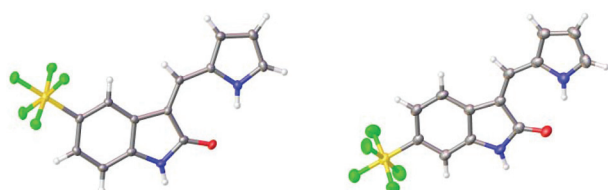


Fig. 3 Solid state structures of 10 and 11.



Fig. 4 Solid state structures of 12a and 12b.

separated by chromatography. Both isomers were characterized in the solid state (Fig. 4).

We tested all synthetic compounds against a panel of kinases in a biochemical assay. Each data point was measured in duplicate (technical replicates). The potencies of compounds that showed appreciable (approx. 50%) inhibition at 1 μ M concentration were established by testing them over a dose range to determine their IC₅₀ values. Additional kinase binding studies were performed vs. a select group of functionally and structurally divergent kinases including AAK1 (Adaptor-associated protein kinase 1), BMP2K (BMP-2-inducible protein kinase, where BMP is bone morphogenic protein), GAK (Cyclin G-associated kinase) and STK16 (Serine/threonine-protein kinase 16) (Table 1). In all assays a control of staurosporine, a known promiscuous kinase inhibitor, was used.

In the case of a number of kinases, *e.g.* VEGFR2 (vascular endothelial growth factor receptor 2) and DYRK2 (Dual-specificity tyrosine phosphorylation-regulated kinase 2), no appreciable inhibition was observed for any of our synthesized compounds, suggesting that we might observe differences in their selectivity, *i.e.* no promiscuity, towards this panel of kinases. Compound 10 bound to BMP2K with an IC₅₀ of 452 nM whereas 11 displayed nM potency vs. PDGFR2 (98 nM) and submicromolar potency vs. VEGFR3 (230 nM). Stereoisomeric 12a and 12b only inhibited DYRK3 in the low micromolar range. The positional isomers 13 and 14 both inhibited VEGFR3 with IC₅₀s of 530 and 18 nM respectively whereas the latter displayed an excellent 3.1 nM IC₅₀ vs. PDGFR α .

The synthesized compounds were next tested in breast cancer and non-transformed breast cell lines. Compounds 10 and 11 potently inhibited MCF7 and T47D breast cancer cell proliferation with GC₅₀ values ranging from 0.35 to 3.8 μ M with compound 11 proving superior to compound 10.

MCF7 and T47D cells are luminal A ER⁺/PR⁺/HER2⁻ cells that would normally be responsive to estrogen and progesterone receptor (ER/PR) antagonists such as tamoxifen and megestrol respectively, but not to human epidermal growth factor receptor 2 (HER2) inhibitors. MDA-MB-231 (abbreviated as MM231) cells are triple negative (ER⁻/PR⁻/HER2⁻) and cannot be treated with hormone receptor and EGFR (HER2) inhibitors, making cancer cells such as these refractory to most treatment strategies. Compounds 10 and 11 may offer advantages for the treatment of ER⁺/PR⁺ cancer cells by poly-



Table 1 Biochemical kinase assays

	Kinase ^a	10	11	12a	12b	13	14	Staurosporine ^c
1	IC ₅₀ (M) STK16 ^b	1.76 × 10 ⁻⁵	1.35 × 10 ⁻⁴	nt	nt	—	—	1.14 × 10 ⁻⁷
2	GAK ^b	3.42 × 10 ⁻⁵	4.76 × 10 ⁻⁷	nt	nt	—	—	1.89 × 10 ⁻⁸
3	BMP2K ^b	4.52 × 10 ⁻⁷	1.87 × 10 ⁻⁴	nt	nt	—	—	3.17 × 10 ⁻⁹
4	AAK1 ^b	1.0 × 10 ⁻⁶	1.0 × 10 ⁻³	nt	nt	—	—	2.47 × 10 ⁻⁹
5 ^d	DYRK3 (h)	—	—	1.7 × 10 ⁻⁶	2.4 × 10 ⁻⁶	—	—	4.5 × 10 ⁻⁸
6	PDGFRα (h)	—	9.8 × 10 ⁻⁸	—	—	—	3.1 × 10 ⁻⁹	1.2 × 10 ⁻⁹
7	FLT-4 (h) (VEGFR3)	—	2.3 × 10 ⁻⁷	—	—	5.3 × 10 ⁻⁷	1.8 × 10 ⁻⁸	7.8 × 10 ⁻¹⁰

^a Unless stated otherwise, performed in the presence of 10 μM ATP. ^b Binding displacement assays have no ATP present. ^c No activity was observed for **10–14** vs. KDR kinase (h) (VEGFR2), PDGFRβ kinase (h); DYRK1a (h); DYRK2a (h); FLT-1 kinase (h) (VEGFR1), where staurosporine positive controls gave IC₅₀s of 2.3 × 10⁻⁹; 2.5 × 10⁻⁹; 3.2 × 10⁻⁸; 8.3 × 10⁻⁷; 2.8 × 10⁻⁸ respectively. ^d Entries 5–7 performed by CEREP (France; <http://www.cerep.fr>). nt – not tested. — insufficiently active for an IC₅₀ determination.

pharmacologically targeting multiple kinases such as the receptor tyrosine kinases and other serine/threonine kinases. Lastly, it is encouraging that normal MCF10A cells were resistant to all inhibitor treatments suggesting these compounds would have a large therapeutic window (Table 2).

Compound **11**, which bears a methylidene indolinone scaffold (Fig. 1), demonstrated its greatest potency against the receptor tyrosine kinase PDGFRα, which adopts an inactive conformation according to X-ray crystallographic analysis (Fig. S1B†); however, an X-ray co-crystal structure containing a methylidene indolinone-based inhibitor (**15**, Fig S1†) bound to the RET kinase domain reveals a type 1 inhibitor binding-mode, or binding to an active kinase conformation (Fig. S1B†). Alignment of **15**-bound RET with the PDGFRα structure reveals gross structural shifts between analogous β-hairpins and α-helices, which is not surprising as the active conformation is generally rigid and condensed and the inactive conformation is generally more open.³⁰ Alignment of the Dasatinib-bound co-crystal structure of Protein-tyrosine kinase 6 (PTK6), a non-receptor tyrosine kinase, with the **15**-bound RET reveals that they share a similar, active conformation (Fig. S1C†). Based on this analysis, it makes sense to use an active kinase conformation, as the above elements (β-hairpin and α-helix) are proximal to the ATP-binding pocket and likely to have an impact on binding mode. However, rather than performing docking studies with RET, we decided that PTK6 would be superior as this kinase has a threonine gatekeeper residue, similar to that of PDGFRα, whereas RET has a valine at the same position. Valine is slightly bigger and more hydrophobic than threonine, lacking a hydroxyl group compared to threo-

nine, and could drastically perturb interactions necessary for **10** and **11**-binding. Furthermore, based on the similarity of **10** and **11** with other type 1 methylidene indolinone inhibitors, we predicted that docking these compounds to an active PTK6 kinase conformation would yield improved binding energies; a result confirmed by docking **10** and **11** to the inactive kinase conformation of PDGFRα (PDB: 5K5X), which reported higher binding energies, and thus less avid binding, for both **10** and **11**.

Against PTK6, both compounds bind in a very similar manner as seen in Fig. 5 (top panel). We found the SF₅ moiety of **10** and **11** to bind deeply in a predominantly hydrophobic



Fig. 5 Docking poses of **10** and **11**. Docking was performed using AutoDock 4.2.6.; Lamarckian Genetic Algorithm empirical free energy scoring function. PDB format files for the ligand and kinase domain were pre-processed using AutoDock Tools 1.5.6.

Table 2 Cellular activity of **10** and **11**

Compound	MCF7	GC ₅₀ ^a , μM T47D	MDA-MB-231	MCF10A
10	4.8 ± 1	0.49 ± 0.4	na	na
11	0.69 ± 0.4	0.35 ± 0.1	na	na

^a The GC₅₀ value was defined as the amount of compound that caused 50% reduction in cellular proliferation in comparison with DMSO-treated control and was calculated using GraphPad Prism version 6 software; na = not applicable.



pocket next to the gatekeeper residue (Fig. 5 top and bottom panels). The amide hydrogen of both compounds interacts with the Met267 backbone; however, note that the attachment of the SF₅ group to position 5 of the oxindole ring forces compound **10** to swing away slightly from the hinge. This may explain why inhibitor **11** is more potent in cells and *in vitro* (PDGFR α & VEGFR3) as the hydrogen bond distance is shorter for the **11** docking-pose, indicative of a stronger interaction.

Conclusion

A small library of SF₅-containing oxindole analogues has been synthesized. Many products were characterized in the solid state and assayed *vs.* a small panel of kinases. Docking studies predicted effective binding of the SF₅ group to a hydrophobic cleft in the kinase and biochemical assays showed little evidence of promiscuity in the range of analogues synthesized. This bodes well for the use of the SF₅ group in medicinal chemistry with compound **14** in particular showing low nM potency against VEGFR3 and PDGFR α kinases.

Experimental

5-(Pentafluorosulfanyl)-1,3-dihydro-indol-2-one and 6-(pentafluorosulfanyl)-1,3-dihydro-indol-2-one were obtained from SpiroChem (<https://spirochem.com/sf5.html>). Ferrocene carboxaldehyde, pyrrole-2-carboxaldehyde and piperidine were obtained from Sigma-Aldrich. Preparative TLC plates were obtained from Analtech. Solvents and reagents were purchased from commercial suppliers and were used without purification. All reactions were performed in a fume hood. NMR spectra were recorded on Varian 500 MHz or 400 MHz spectrometers and chemical shifts are reported in ppm, usually referenced to TMS as an internal standard. LCMS were performed by Shimadzu LCMS-2020 equipped with a Gemini® 5 μ m C18 110 Å column and percentage purities were ran over 30 minutes in water/acetonitrile with 0.1% formic acid (5 min at 5%, 5%–95% over 20 min, 5 min at 95%) with the UV detector at 254 nm. Mass spectrometry: ESI mass spectra were obtained using a Bruker Daltonics Apex III, using Apollo ESI as the ESI source. For EI mass spectra, a Fissions VG Autospec instrument was used at 70 eV. Analyses are for the molecular ion peak [M]⁺ and are given in *m/z*, mass to charge ratio. Elemental analyses were conducted by Stephen Boyer (London Metropolitan University). A CEM Explorer microwave unit was used for microwave reactions (under fumehood) with the hood placed down. The following CCDCs have been deposited for the solid-state structures presented herein: **10** = 154150; **11** = 154151; **12a** = 154152; **12b** = 154153.†

(Z)-3-(1H-Pyrrol-2-yl)methylene-5-pentafluorosulfanylindoline-2-one, **10**

5-(Pentafluorosulfanyl)-1,3-dihydro-indol-2-one (129.6 mg, 0.5 mmol), pyrrole-2-carboxaldehyde (57.06 mg, 0.6 mmol),

ethanol (5 mL) and cat. piperidine (3 drops) were subjected to microwave irradiation by ramping to 150 °C and were held at that temperature for 30 minutes. TLC analysis of the cooled reaction mixture monitored consumption of starting materials. The crude reaction mixture was extracted with ethyl acetate (2 \times 10 cm³) and washed with deionised water (10 mL) and brine (2 \times 10 mL), the organic layer was dried using magnesium sulphate then filtered through a cotton wool plug. The crude mixture was concentrated *in vacuo* and purified using silica gel column chromatography using 3:7 hexane/diethyl ether to give an orange solid. The yield was 105 mg, 65%. Crystallization by mixed solvents, CH₂Cl₂ and hexane, provided orange crystals. ¹H NMR (DMSO-d₆, 500 MHz): δ = 13.22 (1H, s, NH), 11.30 (1H, s, NH), 8.24 (1H, d, *J* = 2.3 Hz, CH), 8.11 (1H, s, CH), 7.65 (1H, dd, *J* = 8.6, 2.2 Hz, CH), 7.44 (1H, d, *J* = 2.2 Hz, CH), 7.02 (1H, d, *J* = 8.6 Hz, CH), 6.92 (1H, d, *J* = 3.6 Hz, CH), 6.41 (1H, dd, *J* = 3.6, 2.2 Hz, CH). ¹³C NMR (DMSO-d₆, 126 MHz): δ = 169.9, 147.5, 141.5, 130.0, 129.5, 127.6, 125.9, 124.7, 122.5, 116.7, 115.2, 112.3, 109.6. HRMS-ESI (*m/z*) found: 337.0431, calc. for [C₁₃H₉F₅N₂OS + H]⁺ 337.0429. Anal. calcd (%) for C₁₃H₉F₅N₂OS: C, 46.43; H, 2.70; N, 8.33; found (%): C, 46.55; H, 2.61; N, 8.21.

(Z)-3-(1H-Pyrrol-2-yl)methylene-6-pentafluorosulfanylindoline-2-one, **11**

6-(Pentafluorosulfanyl)-1,3-dihydro-indol-2-one (129.6 mg, 0.5 mmol), pyrrole-2-carboxaldehyde (57.06 mg, 0.6 mmol), ethanol (5 mL) and cat. piperidine (3 drops) were subjected to microwave irradiation by ramping to 150 °C and were held at that temperature for 30 minutes. TLC analysis of the cooled reaction mixture showed consumption of starting materials. The crude reaction mixture was extracted with ethyl acetate (2 \times 10 mL) and washed with deionised water (10 mL) and brine (2 \times 10 mL), the organic layer was dried using magnesium sulphate then filtered through a cotton wool plug. The crude mixture was concentrated *in vacuo* and purified using silica gel column chromatography using 3:7 hexane/ethyl acetate and trituration with hexane to give brown-orange solid. The yield was 142 mg, 74%. Crystallization in CH₂Cl₂ (DCM) provided orange crystals. ¹H NMR (DMSO-d₆, 500 MHz): δ = 13.31 (1H, s, NH), 11.14 (1H, s, NH), 7.99 (1H, s, CH), 7.81 (1H, d, *J* = 8.6 Hz, CH), 7.53 (1H, dd, *J* = 8.6, 2.0 Hz, CH), 7.48 (1H, s, CH), 7.26 (1H, d, *J* = 2.0 Hz, CH), 6.93 (1H, m, CH), 6.43 (1H, dd, *J* = 3.7, 2.1 Hz, CH). ¹³C NMR (DMSO-d₆, 126 MHz): δ = 169.5, 138.8, 130.2, 130.0, 129.6, 128.3, 123.1, 119.1, 118.7, 114.7, 112.7, 107.0. HRMS-ESI (*m/z*) found: 337.0432, calc. for [C₁₃H₉F₅N₂OS + H]⁺ 337.0429. Anal. calcd (%) for C₁₃H₉F₅N₂OS: C, 46.43; H, 2.70; N, 8.33. Found (%): C, 46.59; H, 2.61; N, 8.17.

5-Pentafluorosulfanyl-3-ferrocenylindolin-2-one, **12a,b**

5-(Pentafluorosulfanyl)-1,3-dihydro-indol-2-one (259.2 mg, 1.0 mmol), ferrocenecarboxaldehyde (256.8 mg, 1.2 mmol), ethanol (10 mL) and cat. piperidine (6 drops) were subjected to microwave irradiation and work-up as above. The crude mixture was concentrated *in vacuo* and purified using prepara-



tive TLC using 3:7 hexane/ethyl acetate to give fraction 1 (purple solid; 160 mg, 35%) and fraction 2 (red solid; 109 mg, 24%). Crystallization of fraction 1 was by mixed solvents (CH₂Cl₂ and hexane) and fraction 2 was by CH₂Cl₂ alone. **(Z)-12a**. ¹H NMR (DMSO-d₆, 500 MHz): δ = 10.84 (1H, s, NH), 8.23 (1H, s, CH), 7.98 (1H, s, CH), 7.68 (1H, d, *J* = 8.6, CH), 6.92 (1H, d, *J* = 8.6 Hz, CH), 5.37 (2H, s, 2CH), 4.69 (2H, s, 2CH), 4.22 (5H, s, Cp). ¹³C NMR (CDCl₃-d, 126 MHz): δ = 167.7, 141.9, 125.1, 119.3, 116.0, 110.0, 108.4, 74.0, 73.3, 70.0, 60.3, 14.2. HRMS-ESI (*m/z*) found: 455.0065, calc. for [C₁₉H₁₄F₅FeNOS]⁺ 455.0060. Anal. calcd (%) for C₁₉H₁₄F₅FeNOS: C, 50.13; H, 3.10; N, 3.08. Found (%): C, 50.22; H, 3.03; N, 3.07. **(E)-12b**. ¹H NMR (DMSO-d₆, 500 MHz): δ = 10.94 (1H, s, NH), 8.30 (1H, s, CH), 7.76 (1H, d, *J* = 8.4, CH), 7.65–7.71 (1H, m, CH), 7.01 (1H, d, *J* = 8.4, CH), 4.79–7.81 (4H, m, 4CH), 4.29 (5H, m, Cp). ¹³C NMR (CDCl₃-d, 126 MHz): δ = 171.1, 141.8, 109.0, 88.2, 72.6, 71.7, 70.2, 60.3, 31.5, 29.6, 22.6, 20.9, 19.0, 14.1, 14.0. HRMS-ESI (*m/z*) found: 455.0064, calc. for [C₁₉H₁₄F₅FeNOS]⁺ 455.0060. Anal. calcd (%) for C₁₉H₁₄F₅FeNOS: C, 50.13; H, 3.10; N, 3.08. Found (%): C, 50.27; H, 3.23; N, 3.10.

(Z)-3-(2,4-Dimethyl-5-((5-pentafluorosulfanyl-2-oxoindolin-3-ylidene)methyl)-1H-pyrrol-3-yl)propanoic acid, 13

5-(Pentafluorosulfanyl)-1,3-dihydro-indol-2-one (106 mg, 0.41 mmol), 3-(5-formyl-1H-pyrrole-3-yl)propanoic acid (97.6 mg, 0.5 mmol), ethanol (6 mL) and piperidine (5 drops) were subjected to microwave irradiation by ramping to 150 °C and were held at that temperature for 30 minutes. TLC analysis of the cooled reaction mixture monitored consumption of starting materials. The crude reaction mixture was concentrated, washed with hexane and CH₂Cl₂ to give a brown solid. The yield was 141 mg, 79%. ¹H NMR (DMSO-d₆, 500 MHz): δ = 13.46 (1H, s, OH), 8.40 (1H, s, NH), 7.86 (1H, s, NH), 7.55 (1H, d, *J* = 8.6 Hz, CH), 6.98 (1H, *J* = 8.6 Hz, CH), 2.77–2.72 (2H, m, 2CH), 2.62 (2H, t, *J* = 7.7 Hz, CH₂), 2.31 (3H, s, CH₃), 2.28–2.22 (2H, s, CH₂), 1.48 (3H, s). ¹³C NMR (DMSO-d₆, 126 MHz): δ = 186.1, 174.6, 170.0, 140.1, 136.8, 132.7, 126.7, 126.3, 123.6, 116.2, 110.4, 109.0, 88.3, 88.2, 35.2, 20.0, 12.5, 10.1. HRMS-ESI (*m/z*) found: 459.0772, calc. for [C₁₈H₁₇F₅N₂NaO₃S]⁺ 459.0772. Anal. calcd (%) for C₁₈H₁₇F₅N₂O₃S: C, 49.54; H, 3.93; N, 6.42. Found (%): C, 49.63; H, 4.04; N, 6.48.

(Z)-3-(2,4-Dimethyl-5-((6-pentafluorosulfanyl-2-oxoindolin-3-ylidene)methyl)-1H-pyrrol-3-yl)propanoic acid, 14

The title compound was prepared by a Knoevenagel condensation reaction. 6-(Pentafluorosulfanyl)-1,3-dihydro-indol-2-one (106 mg, 0.41 mmol), 3-(5-formyl-1H-pyrrole-3-yl)propanoic acid (97.6 mg, 0.5 mmol), ethanol (6 mL) and piperidine 5 drops were subjected to the microwave irradiation by ramping to 150 °C and were held at that temperature for 30 minutes. TLC analysis of the cooled reaction mixture monitored consumption of starting materials. The crude reaction mixture was dried, washed with hexane and CH₂Cl₂ to give a brown solid. The yield was 136 mg, 76%. ¹H NMR (DMSO-d₆, 500 MHz): δ = 13.50 (1H, s, OH), 10.87 (1H, s, NH), 7.90 (1H, d, *J* = 8.6 Hz, CH), 7.74 (1H, s, NH), 7.46 (1H, dd, *J* = 8.6, 2.1 Hz,

CH), 7.24 (1H, d, *J* = 2.1 Hz, CH), 2.78–7.69 (1H, m, CH), 2.66–2.61 (2H, m, CH₂), 2.34–2.27 (6H, m, 2CH₃), 2.25 (1H, s, CH), 1.50 (1H, s, CH). ¹³C NMR (DMSO-d₆, 126 MHz): δ = 174.5, 169.7, 137.8, 133.2, 130.4, 126.9, 123.9, 117.9, 109.8, 88.3, 88.2, 44.4, 35.1, 23.1, 22.5, 20.0, 12.5, 9.96. HRMS-ESI (*m/z*) found: 459.0776, calc. for [C₁₈H₁₇F₅N₂NaO₃S]⁺ 459.0772. Anal. calcd (%) for C₁₈H₁₇F₅N₂O₃S: C, 49.54; H, 3.93; N, 6.42. Found (%): C, 49.70; H, 4.09; N, 6.56.

Conflicts of interest

There are no conflicts to declare.

Acknowledgements

We would like to express our thanks to: the Royal Thai Government, who kindly funded a PhD (S. S.), the European Community's Seventh Framework Programme (FP7/2007–2013) under grant agreement no: PIIF-GA-2011-301062 (C. A. O.). The EPSRC UK National Mass Spectrometry Facility at Swansea University is thanked for MS measurements. The SGC is a registered charity (number 1097737) that receives funds from AbbVie, Bayer Pharma AG, Boehringer Ingelheim, Canada Foundation for Innovation, Eshelman Institute for Innovation, Genome Canada, Innovative Medicines Initiative (EU/EFPIA) [ULTRA-DD grant no. 115766], Janssen, Merck & Co., Novartis Pharma AG, Ontario Ministry of Economic Development and Innovation, Pfizer, São Paulo Research Foundation-FAPESP, Takeda, and Wellcome Trust [092809/Z/10/Z]. The EPSRC is thanked for funding the National Crystallography Service.

References

- 1 J. Zhang, P. L. Yang and N. S. Gray, *Nat. Rev. Cancer*, 2009, **9**, 28–39.
- 2 F. Zuccotto, E. Ardini, E. Casale and M. Angiolini, *J. Med. Chem.*, 2010, **53**, 2681–2694.
- 3 J. C. Uitdehaag, F. Verkaar, H. Alwan, J. de Man, R. C. Buijsman and G. J. Zaman, *Br. J. Pharmacol.*, 2012, **166**, 858–876.
- 4 S. Knapp, P. Arruda, J. Blagg, S. Burley, D. H. Drewry, A. Edwards, D. Fabbro, P. Gillespie, N. S. Gray, B. Kuster, K. E. Lackey, P. Mazzafera, N. C. Tomkinson, T. M. Willson, P. Workman and W. J. Zuercher, *Nat. Chem. Biol.*, 2013, **9**, 3–6.
- 5 M. W. Karaman, S. Herrgard, D. K. Treiber, P. Gallant, C. E. Atteridge, B. T. Campbell, K. W. Chan, P. Ciceri, M. I. Davis, P. T. Edeen, R. Faraoni, M. Floyd, J. P. Hunt, D. J. Lockhart, Z. V. Milanov, M. J. Morrison, G. Pallares, H. K. Patel, S. Pritchard, L. M. Wodicka and P. P. Zarrinkar, *Nat. Biotechnol.*, 2008, **26**, 127–132.
- 6 O. Fedorov, S. Muller and S. Knapp, *Nat. Chem. Biol.*, 2010, **6**, 166–169.



- 7 R. Kumar, M. C. Crouthamel, D. H. Rominger, R. R. Gontarek, P. J. Tummino, R. A. Levin and A. G. King, *Br. J. Cancer*, 2009, **101**, 1717–1723.
- 8 L. Maskell, E. A. Blanche, M. A. Colucci, J. L. Whatmore and C. J. Moody, *Bioorg. Med. Chem. Lett.*, 2007, **17**, 1575–1578.
- 9 J. Spencer, B. Chowdhry, S. Hamid, A. Mendham, L. Male, S. Coles and M. Hursthouse, *Acta Crystallogr., Sect. C: Cryst. Struct. Commun.*, 2010, **66**, o71–o78.
- 10 R. R. Khanwelkar, G. S. Chen, H. C. Wang, C. W. Yu, C. H. Huang, O. Lee, C. H. Chen, C. S. Hwang, C. H. Ko, N. T. Chou, M. W. Lin, L. M. Wang, Y. C. Chen, T. H. Hseu, C. N. Chang, H. C. Hsu, H. C. Lin, Y. C. Shih, S. H. Chou, H. W. Tseng, C. P. Liu, C. M. Tu, T. L. Hu, Y. J. Tsai and J. W. Chern, *Bioorg. Med. Chem.*, 2010, **18**, 4674–4686.
- 11 K. Lv, L. L. Wang, M. L. Liu, X. B. Zhou, S. Y. Fan, H. Y. Liu, Z. B. Zheng and S. Li, *Bioorg. Med. Chem. Lett.*, 2011, **21**, 3062–3065.
- 12 A. Sartori, E. Portioli, L. Battistini, L. Calorini, A. Pupi, F. Vacondio, D. Arosio, F. Bianchini and F. Zanardi, *J. Med. Chem.*, 2017, **60**, 248–262.
- 13 L. Sun, C. Liang, S. Shirazian, Y. Zhou, T. Miller, J. Cui, J. Y. Fukuda, J.-Y. Chu, A. Nematalla, X. Wang, H. Chen, A. Sistla, T. C. Luu, F. Tang and J. W. Tang, *J. Med. Chem.*, 2003, **46**, 1116–1119.
- 14 C. L. Tourneau, E. Raymond and S. Faivre, *Ther. Clin. Risk Manage.*, 2007, **3**, 341–348.
- 15 C. Adams, D. J. Aldous, S. Amendola, P. Bamborough, C. Bright, S. Crowe, P. Eastwood, G. Fenton, M. Foster, T. K. P. Harrison, S. King, J. Lai, C. Lawrence, J.-P. Letaltec, C. McCarthy, N. Moorcroft, K. Page, S. Rao, J. Redford, S. Sadiq, K. Smith, J. E. Souness, S. Thurairatnam, M. Vine and B. Wyman, *Bioorg. Med. Chem. Lett.*, 2003, **13**, 3105–3110.
- 16 J. Spencer, J. Amin, S. K. Callear, G. J. Tizzard, S. J. Coles, P. Coxhead and M. Guille, *Metallomics*, 2011, **3**, 600–608.
- 17 J. Spencer, A. P. Mendham, A. K. Kotha, S. C. Richardson, E. A. Hillard, G. Jaouen, L. Male and M. B. Hursthouse, *Dalton Trans.*, 2009, 918–921.
- 18 H. Bregman, D. S. Williams, G. E. Atilla, P. J. Carroll and E. Meggers, *J. Am. Chem. Soc.*, 2004, **126**, 13594–13595.
- 19 L. Zhang, P. Carroll and E. Meggers, *Org. Lett.*, 2004, **6**, 521–523.
- 20 J. E. Debreczeni, A. N. Bullock, G. E. Atilla, D. S. Williams, H. Bregman, S. Knapp and E. Meggers, *Angew. Chem., Int. Ed.*, 2006, **45**, 1580–1585.
- 21 E. Meggers, *Chem. Commun.*, 2009, 1001–1010.
- 22 P. Beier and T. Pastyrikova, *Beilstein J. Org. Chem.*, 2013, **9**, 411–416.
- 23 B. Stump, C. Eberle, W. B. Schweizer, M. Kaiser, R. Brun, R. L. Krauth-Siegel, D. Lentz and F. Diederich, *ChemBioChem*, 2009, **10**, 79–83.
- 24 G. C. Moraski, R. Bristol, N. Seeger, H. I. Boshoff, P. S.-Y. Tsang and M. J. Miller, *ChemMedChem*, 2017, **12**, 1108–1115.
- 25 P. R. Savoie and J. T. Welch, *Chem. Rev.*, 2015, **115**, 1130–1190.
- 26 M. F. Sowaileh, R. A. Hazlitt and D. A. Colby, *ChemMedChem*, 2017, **12**, 1481–1490.
- 27 P. Beier, G. Iakobson and M. Pošta, *Synlett*, 2013, 855–859.
- 28 J. Spencer, J. Amin, P. Coxhead, J. McGeehan, C. J. Richards, G. J. Tizzard, S. J. Coles, J. P. Bingham, J. A. Hartley, L. Feng, E. Meggers and M. Guille, *Organometallics*, 2011, **30**, 3177–3181.
- 29 S. J. Coles and P. A. Gale, *Chem. Sci.*, 2012, **3**, 683–689.
- 30 A. P. Kornev, N. M. Haste, S. S. Taylor and L. F. Eyck, *Proc. Natl. Acad. Sci. U. S. A.*, 2006, **103**, 17783–17788.

